Journal of Materials and Environmental Sciences
ISSN : 2028-2508

JMES, 2017 Volume 8, Issue 4, Page 1301-1311

http://www.jmaterenvironsci.com /

The photocatalytic degradation of methylene bleu over TiO_2 catalysts supported on hydroxyapatite

A. El ouinani*[a], I. Boumanchar[a,b], M. Zbair[a], Y. Chhiti[b], A. Sahibed-dine[a], F. Bentiss[a,c], M. Bensitel[a]

[a]*Laboratory of Catalysis and Corrosion of Materials, Department of Chemistry P.O Box 20, 24000 , University of Chouaïb Doukkali, Faculty of sciences of El Jadida , Morocco*

[b]*Engineer Science Laboratory for Energy LabSIPE, National School of Applied Sciences, University of Chouaïb Doukkali of El Jadida, Morocco.*

[c]*UMET-ISP, CNRS UMR 8207, ENSCL, P.O Box 90108, F-59652 Villeneuve d'Ascq Cedex, University of Lille, France*

Received 14 Oct 2016,
Revised 15 Dec 2016,
Accepted 22 Dec 2016

Keywords
- ✓ Photocatalytic degradation;
- ✓ TiO_2-HAp catalyst;
- ✓ Hydroxyapatite;
- ✓ Methylene bleu;
- ✓ Heterogeneous catalysis.

amal.elouinani@gmail.com
asahibeddine@gmail.com

Abstract

This paper investigated the photocatalytic degradation of Methylene Bleu (MB) (as one of model compounds of organic dyes in wastewaters) over TiO_2 catalyst supported on Hydroxyapatite (HAp). HAp was synthesized by the double decomposition method; thereafter titanium oxide (TiO_2) was supported on this base by the chemical wet impregnation (WI) method at different TiO_2 amounts. The characterization of the catalysts revealed that the performance of the catalyst is related to the interaction between TiO_2 active phase and the support. Catalysts with different percentages of TiO_2 have been explored. 40 wt.%TiO_2/HAp sample present the optimal photocatalytic activity. This result proves that combining HAp and TiO_2 improve effectively the photocatalytic activity, and therefore improve the degradation of the organic pollutant MB more than that of pure TiO_2 under ultraviolet (UV) irradiation.

1. Introduction

One of the most severe problems confronting people throughout the world is inadequate access to remove organic and inorganic pollutants from wastewaters [1]. The presence of dyes in wastewaters has been recognized as one of the most serious environmental dangerous substances, which can cause adverse effects on the endocrine system [2]. In recent years, with the growing necessity for clean water, many treatment strategies have been investigated for removing the pollutants of dyes [3]. Among those strategies, photocatalytic oxidations have attracted extensive attention as emerging successful technologies [4]. Up to now, TiO_2 photocatalysts have been widely used as an excellent materiel for the photocatalytic processes, due to its chemical stabilities, low cost and its high activity [5]. However, one of the main drawbacks is very weak adsorption ability of TiO_2 to some dyes [3,6,7] and other organic pollutants [8,9]. Thus, various methods have been explored to convert the TiO_2 adsorption from the ultraviolet to the visible region by modification [10,11] or by doping with several transition metals, such as cerium [12], tungsten [13,14], molybdenum [15–18], gold [19], nickel [20–22] and platinum [23] ions.

With the growing necessity for biomaterials, hydroxyapatite $Ca_{10}(PO_4)_6(OH)_2$, abbreviated as HAp has attracted much attention, due to its excellent biocompatibility and biological similarity of natural bone [24]. HAp is not only a main component of hard tissues, such as bones and teeth, but an excellent adsorbent for adsorption and separation of biomolecules, pollutants and heavy metal ions [25-27]. It has been reported that TiO_2 and HAp represent a good combination to form a composite which has a good mechanical properties [28], an excellent ability to adsorb and decompose organic dyes and it is considered to be good for both environmental processes and various industrial purposes including fertilizer production, water purification and degradation of pollutants [29-32].

In the present study, TiO_2/HAp samples were successfully synthesized using double decomposition and WI methods. The effect of TiO_2 additive on the structural, morphological and textural properties has been investigated. The samples were evaluated for the degradation of MB under UV irradiation.

2. Experimental

2.1. Materials

The reagents used in the experiments are: Calcium nitrate [$Ca(NO_3)_2$,$4H_2O$], diammonium hydrogenophosphate [$(NH_4)_2HPO_4$], ammonium hydroxide (25%), MB (λ_{max}= 664 nm) and titanium tetra isopropoxide ($Ti(OC_3H_7)_4$, 96% purity).

The solutions were prepared by using pure distilled water. All the chemicals were used as received without any further purification. Characteristics and molecular structures of MB dye are shown in Table 1 and Figure 1, respectively.

Table 1: *Physicochemical properties of methylene bleu*

Contaminant name	Linear formula	Molecular weight (g/mol)	Contents (%)	λ_{max} (nm)	Class
Methylene bleu	$C_{16}H_{18}ClN_3S.3H_2O$	373.90	97	664	Heteropolyaromatic dye

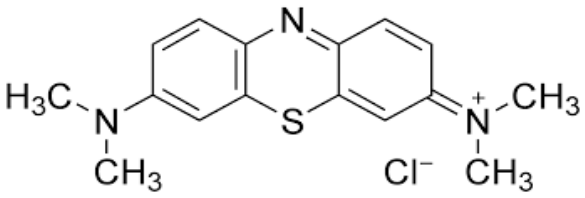

Figure 1: Molecular structure of MB.

2.2. Synthesis of HAp support

The HAp $Ca_{10}(PO_4)_6(OH)_2$ was prepared by double decomposition method. In a typical experiment, a solution of calcium nitrate and diammonium hydrogenophosphate were used as calcium and phosphate sources respectively. The HAp was prepared by taking the above compound separately and then mixed with distilled water with the molar ratio of 1.67 which is the stoichiometric molar ratio of HAp, under vigorous stirring the calcium solution was added drop wise to the solution of the phosphate over a period of 3 hours. The solution is carried in a nearby temperature of 80°C. The pH of the solution was increased to 10 by adding ammonium hydroxide to produce a milky white precipitate, which was then stirred and boiled for 30 min under agitation, after filtration the precipitate was washed thoroughly, dried at 100°C over night and then calcined at 500°C for 2h with a temperature rise of 5°C min^{-1}.

2.3. Synthesis of x% TiO_2/HAp photocatalysts

TiO_2/HAp catalyst was prepared from HAp and titanium tetra isopropoxide (TTIP) by using a standard WI method. 1g of HAp carrier and 0.5 ml of distilled water were added in 50ml of absolute alcohol in 250 ml beaker to get a suspension, which was stirred at room temperature for 2h. After that, the appropriate amount of TTIP with different TiO_2 proportion of 0, 10, 20 and 40 wt.% was introduced into the aforementioned dispersive solution, followed by continuous stirring for 3h. Product was washed several times with distilled water and then dried at 120 °C over night. The samples were calcined at 500°C for 5h with a temperature rise of 5°C min^{-1}.

2.4. Characterization methods

The catalysts were characterized by:

- X-ray diffraction analysis (XRD) using a Bruker- eco D8 Advance diffractometer with Cu-K_α radiation source (λ = 1.5418 Å). The 2θ angles that were scanned ranged from 10 to 70°. Diffraction patterns were compared to International Center for Diffraction Data (ICCD) for identification of crystalline phases. The crystallite size of the active phase and the support was estimated using the Scherrer formula:

$$D = \frac{K\lambda}{\beta c \times \cos\Theta} \quad (1)$$

Where k is the shape factor (k = 0.94) and λ is the wavelength of X-ray; Θ is the Bragg angle and β_c is the corrected line broadening defined as Full Width at Half Maximum (FWHM).

- Fourier transformation infrared (FT-IR) spectra of samples, on KBr pellets, were recorded by Fourier transform infrared (Shimadzu. FTIR-8400S) spectrophotometer in the range of 400 –4000cm^{-1}.
- The thermal analyses are made with the TA instrument balance, model SDT 2966. It allows realizing simultaneously differential thermal analysis (ATD) and thermogravimetric analysis (ATG) behavior of the as-prepared samples under air atmosphere in the temperature range of 25–800 °C and with heating rate of 5 °C/min.
- Morphological characterization and chemical composition of the TiO_2/HAp samples were performed using Scanning Electron Microscopy (SEM) Hitachi S-3400N equipped with an Energy Dispersive X-Ray Spectroscopy (EDS) (Noran with a silicon drift detector). To get a clear insight into the microstructures, transmission electron microscopy (TEM) was performed by using a TEM, Detector: SUTW-Sapphire.

2.5. Photocatalytic experiment

The photocatalytic activity was evaluated in a cylindrical metal reactor at room temperature, it is constituted of six UV lamps; 3 UVA and 3 UVB lamps, each has a low pressure mercury of (8W). The wavelength of maximum of the light sources of the lamps is 450 nm. 20 ml of MB aqueous solutions (MB concentration 10 ppm (part per million)) and 20 mg of TiO_2/HAp catalyst powders were placed in the glass vessel, which formed a suspension under stirring. For comparison, all the experiments were carried out under the identical conditions. The mixture was stirred first in dark for 30 min to evaluate the adsorption-desorption equilibrium, UV light irradiation was turned on. Samples were taken at given time intervals and centrifuged at 4000 round per minute (rpm) for 3 min. The changes of MB concentration with UV irradiation were analyzed using a V-1200 spectrophotometer.

3. Results and discussion

3.1. X-ray diffraction study

Figure 2 shows the XRD patterns of TiO_2/HAp composites with different amounts of TiO_2 (0, 10, 20 and 100 wt.%). The XRD pattern (curve a) for pure HAp shows diffraction peaks at 2Θ = 25.75°, 31.82°, 32.9°, 34.2°, 39.8°, 43.05° and 49.46° are consistent with the (002), (211), (300), (202), (310), (113) and (213) Bragg reflections of HAp respectively.

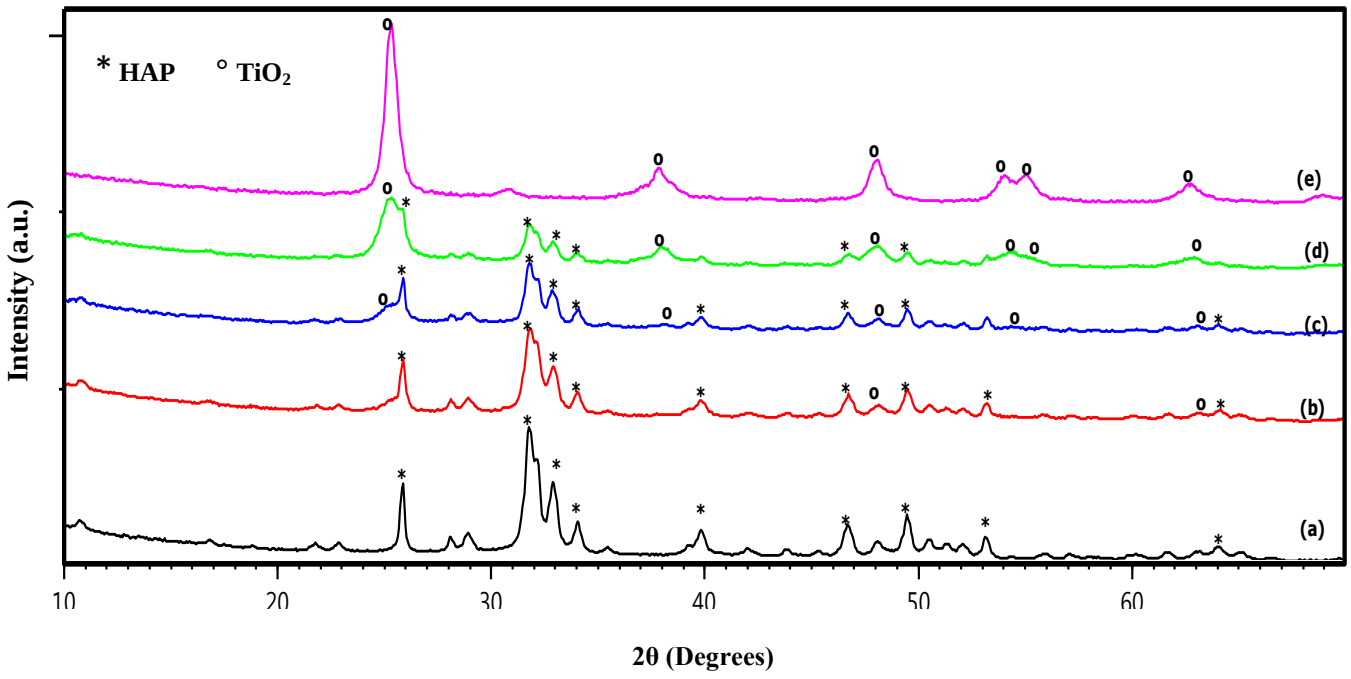

Figure 2: XRD pattern of HAp/TiO_2 samples: (a) pure HAp, (b) 10% TiO_2, (c) 20% TiO_2, (d) 40% TiO_2, and (e) pure TiO_2.

All the diffraction peaks could be readily indexed with the pure hexagonal phase [space group: $P6_{3/m}$], which in agreement with the bulk HAp crystals (JCPDS 09-0432) (Joint Committee on powder Diffraction Standards) [33]. While in pure TiO_2 (curve e) the XRD peaks at 2Θ = 25.2°, 37.8°, 48.1°, 54°, 55.1°, 62.7° and 69° can be exactly indexed to the diffraction of (101), (004), (200), (105), (211), (204) and (220) planes of anatase phase TiO_2 (JCPDS 21-1272) [34]. The peak intensity of anatase increases with the increase of TiO_2 amount in the TiO_2/HAp samples (curves b-d). While the intensity of HAp peak decreases. On the other hand, no new phase was detected. The absence of additional diffractions in x%TiO_2/HAp samples indicated that TiO_2 was highly dispersed throughout the surface of HAp phase.

The average crystallite size of the prepared catalysts and support was estimated using the XRD data by the Scherrer equation. After the addition of 10%, 20% and 40% of TiO_2, an increase of the average crystallite size of the catalysts has been observed, as shown in Figure 3.

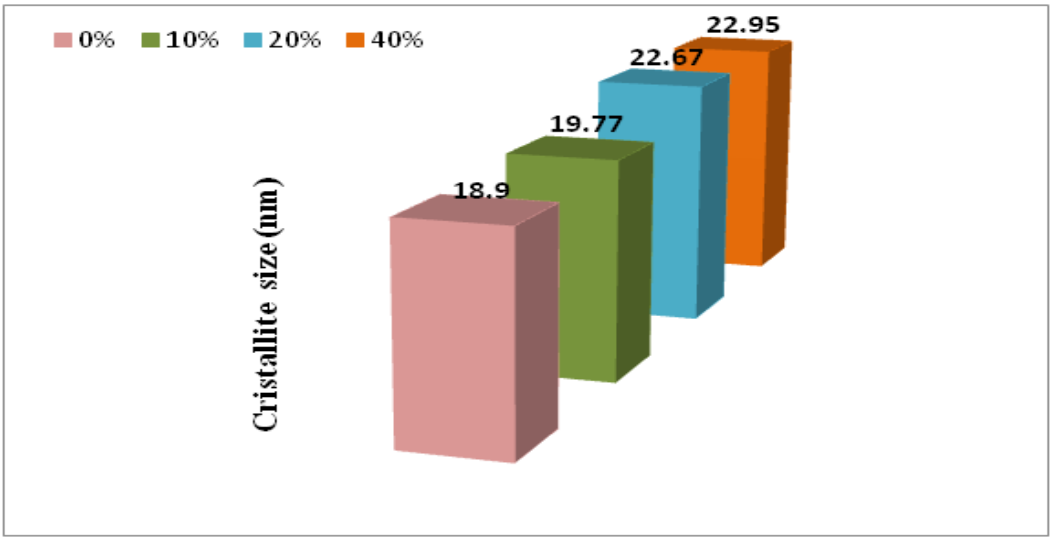

Figure 3: Estimated average particle sizes of the crystallite with different amounts of TiO_2.

3.2. DTA–TGA study

The thermal stability of the pre-calcined HAp-based catalysts was examined by TGA-DTA data presented in Figure 4.

The TGA measurements were conducted on the as synthesized HAp samples after the drying step in furnace. The slight decrease in weight for all the samples at temperature from 25 to 380 °C is assigned to the evaporation of water bound to the catalyst surface or decomposition of adsorbed ammonium or nitrate ions used in the catalyst synthesis. Whereas the second weight loss is noticed in the temperature range of 400–700°C. This is caused by the structure decomposition such as dehydroxylation given that the temperature approaches the thermal stability limit of the HAp material which is in agreement with the results reported in literature [35]. The DTA pattern shows an exothermic band centered around 300°C, which is attributed to the decomposition of nitrates species. According to TGA curves, the weight deduction of 7.9%, 8.4% and 9.8% were obtained for HAp, 20%TiO_2/HAp and 40%TiO_2/HAp catalysts, respectively. These results show a smaller weight loss in TiO_2/HAp. The weight loss values of different catalysts are shown in Table 2.

3.3. FT-IR analysis

Figure 5 illustrates FT-IR results of synthesized HAp and TiO_2 loading HAp samples (10, 20 and 40 wt. % TiO_2) in the spectral region from 400 to 4000 cm^{-1}. The wavenumber of bands and their assignments are summarized in Table 3.

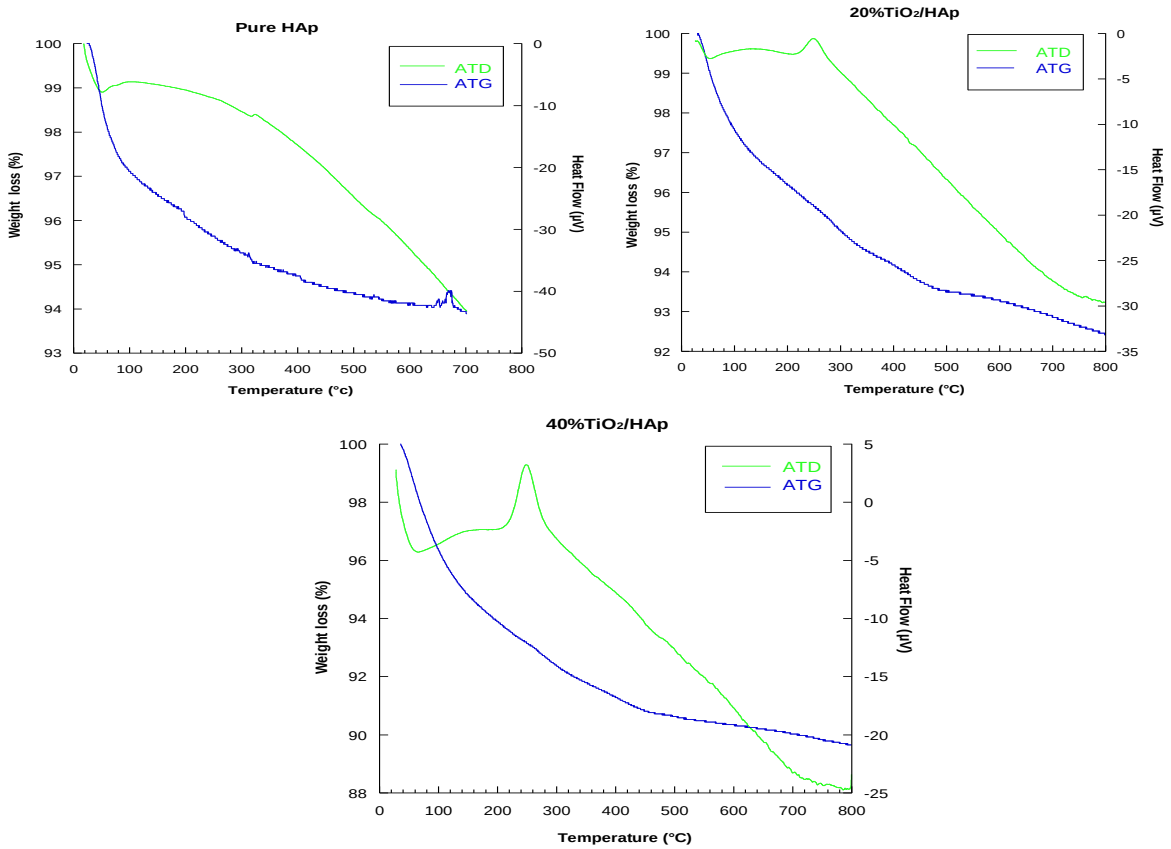

Figure 4: TGA–DTA analysis of the samples.

Table 2: *Weight loss values of Pure HAp and TiO_2/HAp catalysts.*

Samples	Weight loss (%)		
	Δ_{m1}	Δ_{m2}	$\Delta_{m\ total}$
HAp	5.5	2.4	7.9
20%TiO_2/HAp	6.3	2.1	8.4
40%TiO_2/HAp	7.6	2.2	9.8

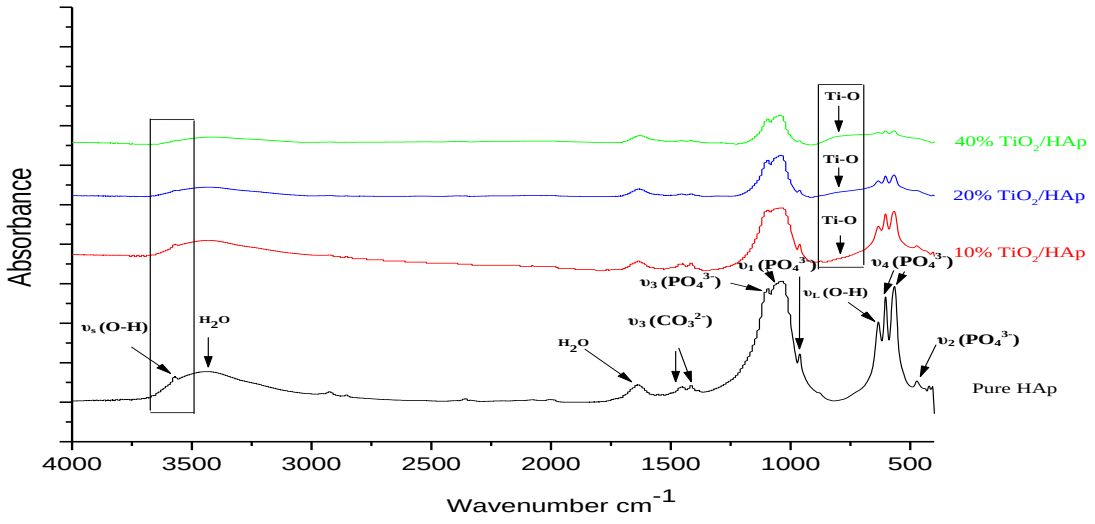

Figure 5: FT-IR spectra obtained from various TiO_2/HAp samples: pure HAp, 10% TiO_2/HAp, 20% TiO_2/HAp, 40% TiO_2/HAp and pure TiO_2.

The infrared spectra of HAp and TiO_2/ HAp catalysts (Figure 5) shows all absorption bands characteristic for HAp which is in agreement with the results reported in literature [36].

- For PO_4^{3-} group, the υ_1 vibration (symmetric stretching) occurred at 962 cm^{-1}, the υ_3 vibration (asymmetric stretching) centered at 1034 and 1099 cm^{-1} (symmetric stretching), while υ_4 vibration (asymmetric bending) located at 563 and (symmetric bending) centered at 602 cm^{-1}.
- For the OH^- group of HAp, the peaks at 632 and at 3575 cm^{-1} are characteristic of the vibrational mode of OH^- groups, suggesting the presence of hydroxyl groups.
- The bending mode of H_2O bond at 1636 cm^{-1} as well as its stretching mode at 3450 cm^{-1}.
- Adsorption bands available at 1411 and 1451 cm^{-1} correspond to carbonate adsorption. A possible explanation for the presence of carbonates ions in the structure of TiO_2/HAp catalysts is that atmospheric CO_2 might have been adsorbed at ambient temperature.
- The absorption peaks at 746 cm^{-1} are the characteristic vibration peaks of the bond Ti-O, which confirms the presence of titania phase. The retaining of Ti-O bond increases as the amount of TiO_2 in the samples increases.
- Concerning PO_4^{3-}, It can be seen from this figure that the intensities of (PO_4^{3-}) adsorption bands at 563 and 1034 cm^{-1} decreases when the amount of TiO_2 in the samples increases. Also, it can be noticed that the peaks at 3575 identified as OH^- adsorption bands disappear when the amount of TiO_2 loading on the catalyst increased.

Table 3: *IR bands assignments of HAp and TiO_2/HAp catalysts*

Mode	HAp	10% TiO_2/HAp	20% TiO_2/HAp	40% TiO_2/HAp
υ_1 (PO_4^{3-})	962	962	-	-
υ_2 (PO_4^{3-})	472	471	-	-
υ_3 (PO_4^{3-})	1034	1034	1041	1041
υ_3 (PO_4^{3-})	1099	1099	1093	1093
υ_4 (PO_4^{3-})	563	563	563	563
υ_4 (PO_4^{3-})	602	602	602	602
υ_3 (CO_3^{2-})	1411	1414	1414	1414
υ_3 (CO_3^{2-})	1451	1453	1453	1453
υ_L (O-H)	632	634	634	630
H_2O	1636	1636	1636	1636
υ_s (O-H)	3575	3568	-	-
H_2O	3450	3452	3450	3450
υ (Ti-O)	-	750	746	746

3.4. SEM-EDS analysis

SEM and EDS were used to reveal the morphologies and elemental distribution of different phases. Figure 6 illustrates SEM micrographs and EDX patterns of HAp, 10% TiO_2/HAp, 20% TiO_2/HAp and 40% TiO_2/HAp. The microstructure of HAp is found to be almost like quasispherical of size ranging from 20 to 40 nm (Figure 6a). Figure 6b shows the microstructure of HAp with 20 wt.% of TiO_2. The addition of 20 wt.% of TiO_2 on HAp leads to the formation of longer HAp needles due to the heterogeneous nucleation. The size of these needles is about 50-70 nm. Further increase in the TiO_2 amount of to 40 wt.% (Figure 6c) resulted the deposition of spherical TiO_2 nanoparticles with a diameter of 20-30 nm like pearls densely inlaying in the ravines of HAp carrier surface.

The elemental composition of the catalysts was examined by SEM-EDS (Figure 6), the analysis revealed the presence of Ca, P, O of HAp Ti, O of TiO_2 compounds respectively. TiO_2 clearly appears in the Figures 6b and 6c confirming the incorporation of TiO_2 on HAp, which is also evident from the XRD analysis.

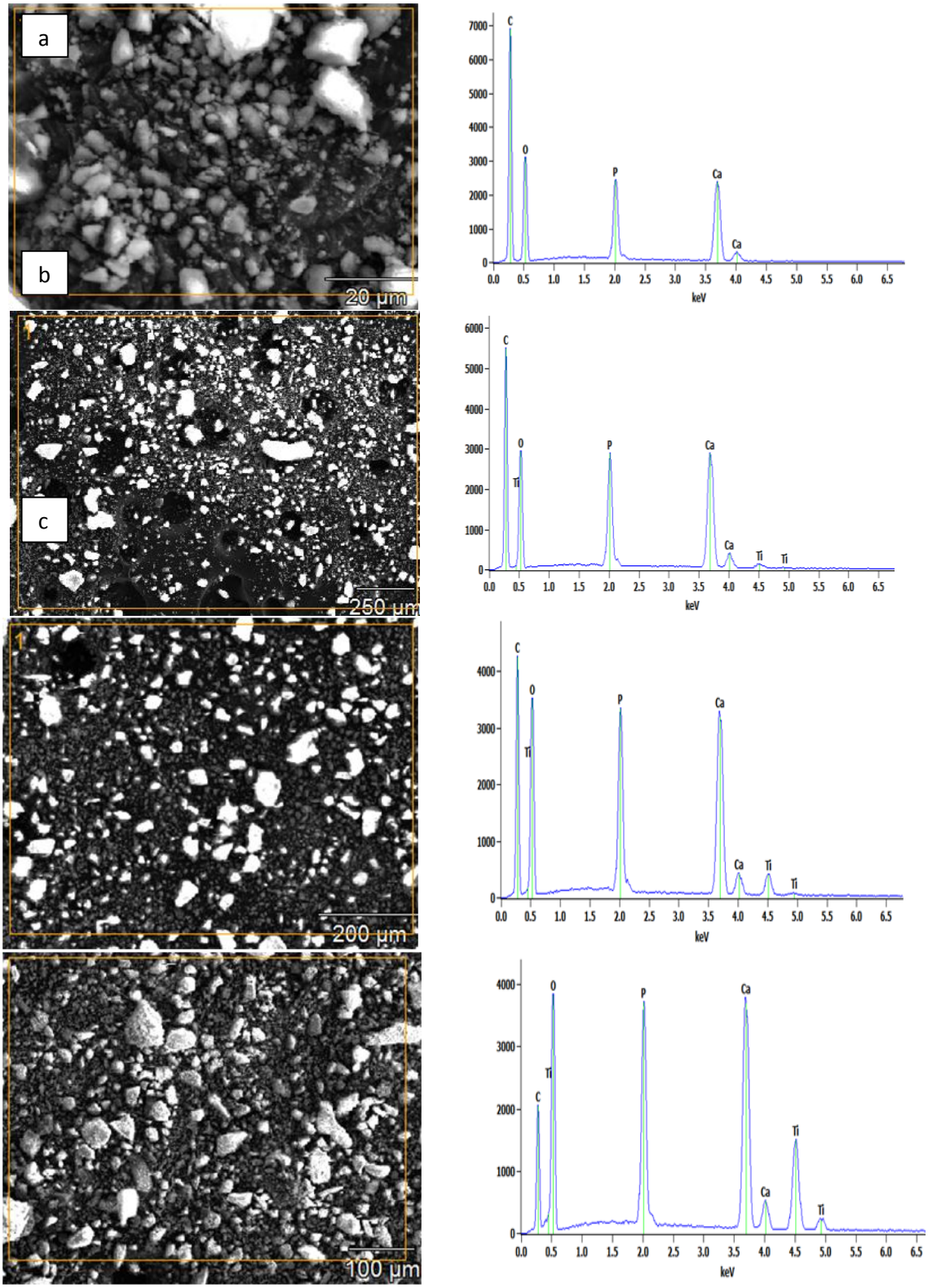

Figure 6: SEM micrographs and EDS spectra of the catalysts: (a) Pure HAp, (b) 10%TiO_2/HAp, (c) 20%TiO_2/HAp and (d) 40% TiO_2/HAp.

3.5. Transmission electron microscopic analysis

To confirm the morphology of the nancomposites, TEM was performed. The TEM micrographs of pure HAp and TiO_2/HAp nancomposites with (10, 20, and 40 wt.% TiO_2) are shown in Figure 7. From the TEM micrographs it can be seen that the amount of TiO_2 in the samples had an influence on the aspect of crystal particles in catalysts prepared. The microstructure showed that HAp exists as needles particles in the range of 20-40 nm (Figure 7a). An increase of 10% of the amount of TiO_2 in the TiO_2/HAp catalyst doesn't cause a large

change in the morphology of the catalyst. Furthermore, in the case of 20 wt.% TiO_2, it seems that increasing in TiO_2 amount creates sphere on the surface of HAp needles (Figure 7b). The addition of 40 wt.% of TiO_2 induces the growth of HAp needles but with rapid increase in deposition of spherical TiO_2 nanoparticles on the surface of HAp, which is in agreement with the results reported in literature [37,38].The impregnation method maintains the original morphology of HAp with increase in length of the needles during the preparation by hydrolyzing Ti-complex. During the hydrolysis, The TiO_2 goes into the HAp and increases the size of the needles and it is confirmed through our XRD measurements.

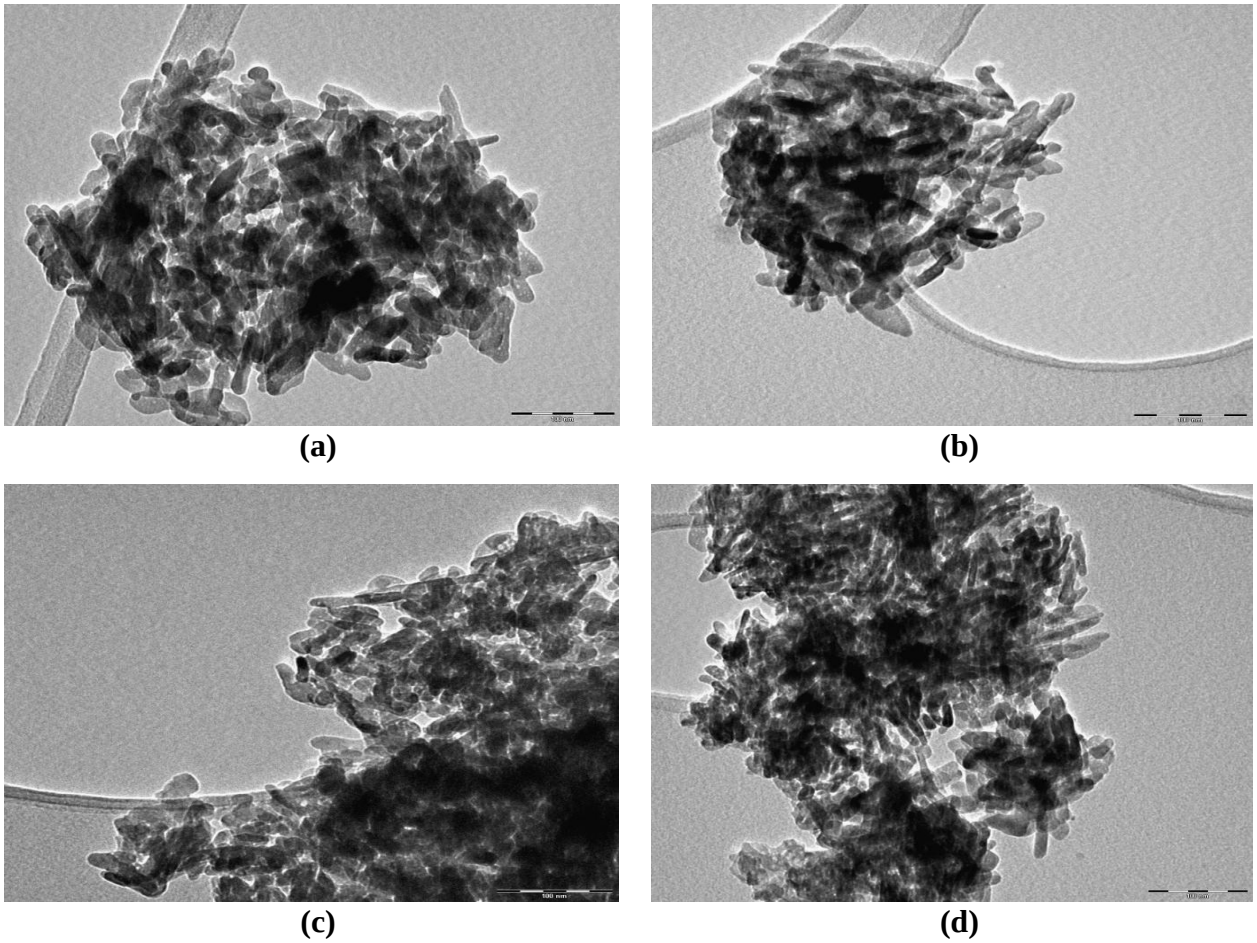

Figure 7: TEM image of the catalysts (a) Pure HAp, (b) 10%TiO_2/HAp, (c) 20%TiO_2/HAp and (d) 40%TiO_2/HAp.

3.6. Photocatalytic activity

The photocatalytic activity degradation under UV irradiation of for MB dye from aqueous solutions has been conducted under HAp, TiO_2/HAp and pure TiO_2. 10 ppm of MB in 20 ml of aqueous solution, initially at pH=6,91 and at room temperature, irradiated during 30 min without illumination and during 70 min under UV irradiation. The samples were taken out for every 10 min to determine the rate of degradation. Fig.8 shows that with the pure HAp no significant degradation of MB is observed under UV irradiation (λ=664 nm) because hydroxyapatite is not an efficient catalyst for photooxidation [38]. However, the increase of TiO_2 amount enhances significantly the rate of decomposition, the maximum degradation is observed at 40 wt.% TiO_2 which much better than that of pure TiO_2 powders.

A possible explanation is that the illumination of TiO_2/HAp by UV light changes the electronic state of the surface PO_4^{3-} group and create a vacancy on HAp, and on the other hand when TiO_2 is irradiated with UV light, electrons in the valence band (VB) are transferred to the conduction band (CB) leading to the formation of the same number of holes in the VB (Eq. (2)).

$$TiO_2 + h\upsilon \rightarrow e^- + h^+ \quad (2)$$

Superoxide anion radicals $O_2^{\cdot-}$ are formed when the electron in the CB react with O_2 which oxidize the organic compounds (Eq. (3)).

$$e^- + O_2 \rightarrow O_2^{\cdot-} \quad (3)$$

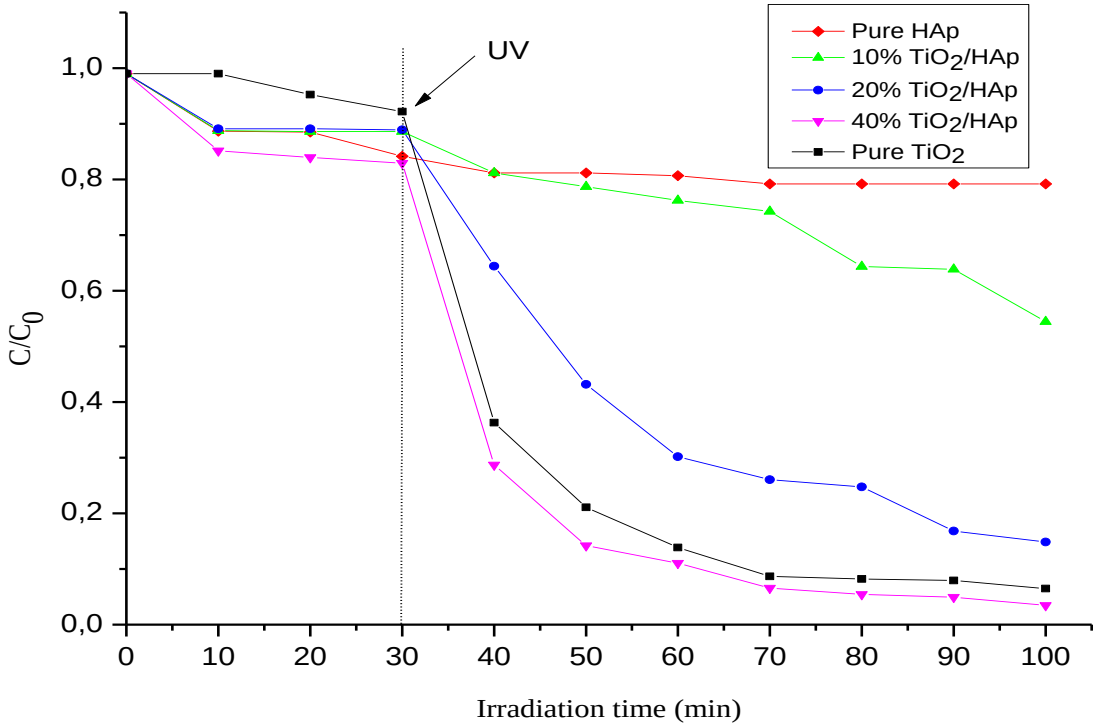

Figure 8: Kinetics of MB dye photodegradation from aqueous solutions with : pure HAp, 10% TiO_2/HAp, 20% TiO_2/HAp, 40% TiO_2/HAp and pure TiO_2 powder.

The VB hole reacts with the adsorbed water or hydroxyl anions to produce hydrogen peroxide (Eqs. (4) and (5)).

$$h^+ + H_2O \rightarrow OH^{\cdot} + H^+ \quad (4)$$

$$h^+ + OH^- \rightarrow OH^{\cdot} \quad (5)$$

This further splits and produces hydroxyl radicals, which is a powerful oxidizing agent and attacks organic molecules adsorbed onto the catalyst present in solution [39]. However, the highest catalytic activity is due in a large part to the extended near-visible absorption of the anatase phase, followed by a rapid electron transfer between the two phases, anatase and HAp. Comparative experimental results just indicate that the existence of HAp with excellent adsorption capacity can help to enhance the photocatalytic activity of TiO_2.

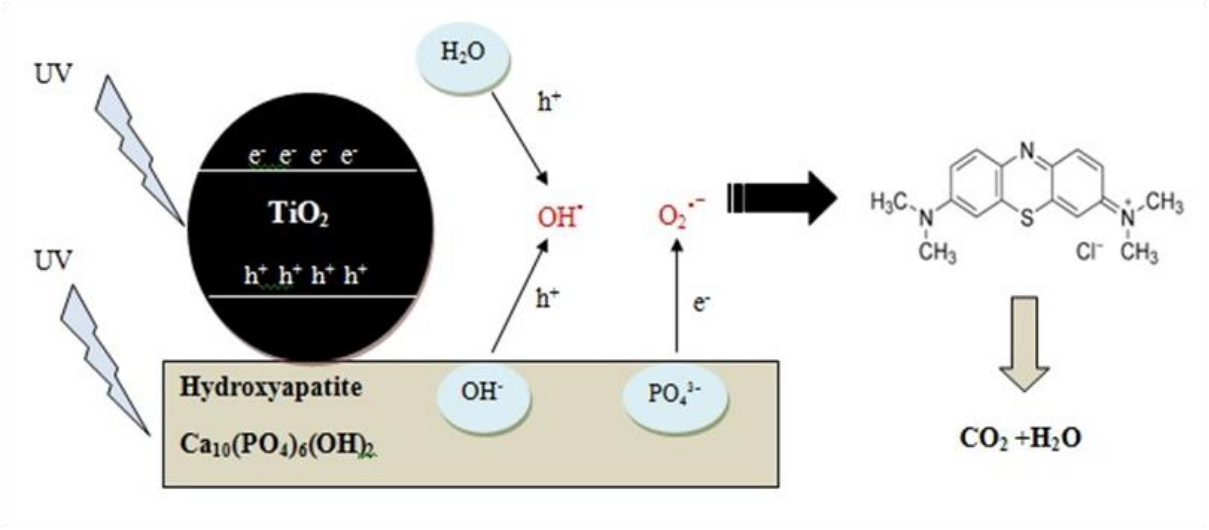

Figure 9: The pictorial representation of UV- illuminated Wt% TiO_2 supported HAp for degradation process of MB.

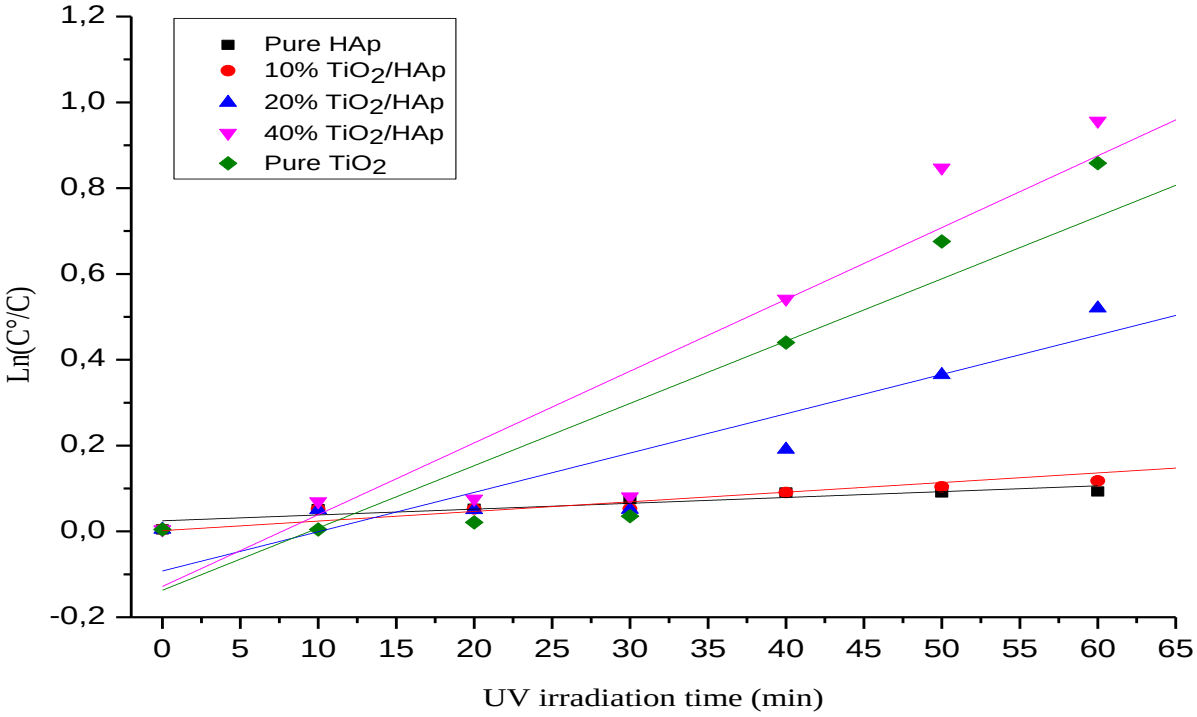

Figure 10: Pseudo-first-order linear plots of Ln (C0/C) vs. irradiation time for the degradation kinetics of molecule under different TiO_2 contents and UV irradiation.

In the Figure 10, it can be seen that the photodegradation reactions of MB obeyed to a pseudo-first-order kinetic model [40]. The results were nearly consistent with the linear equation :

$$\mathbf{Ln\ (C_0/C) = k_{app}.t}$$

where C is the concentration of solution, C_0 is the initial concentration at t=0 and k_{app} is the apparent rate constant. The linear plots of Ln (C_0/C) were plotted as a function of the irradiation time t (min) with MB.

Table 4: *Apparent constants kapp and linear regression coefficients of samples*

Catalysts	K_{app} (min^{-1})	R^2
Pure HAp	0.00136	0.918
10% TiO_2/HAp	0.00224	0.966
20% TiO2/HAp	0.00916	0.989
40%TiO2 /HAp	0.01673	0.989
Pure TiO2	0.01452	0.967

The apparent rate constants k_{app} values calculated from the slopes of the lines and the coefficient of linear regression were calculated and summarized in the table 4 as a function of the catalyst loading. It can be noticed that the rate constant of the catalysts is 0.00136, 0.00224, 0.00916, 0.01673 and 0.01452 for pure HAp, 10%TiO_2/HAp, 20%TiO_2/HAp, 40TiO_2/HAp and pure TiO_2, respectively, was increased with the increase of TiO_2 loading and shows a maximum at 40% TiO_2/HAp.

Conclusions

The photocatalysis is one of the most promising routes for the degradation of organic dyes in wastewaters. MB has been selected as representative model component of organic dyes pollutant. The photocatalytic activity of titanium oxide supported on hydroxyapatite has been investigated.. The results have shown that the addition of TiO_2 on HAp actuates the growth of the nanorods by heterogeneous nucleation. The TiO_2 doping enhances the photocatalytic activity. Catalysts with different percentages of TiO_2 have been explored (0, 10, 20 and 40 wt.%). 40 wt.% TiO_2/HAp sample present the optimal photocatalytic activity and allows a better degradation of the pollutant (MB) under UV irradiation.

References

1. Shannon M.A., Bohn P.W., Elimelech M., Georgiadis J.G., Mariñas B.J., Mayes A.M., *Nature* 452 (2008) 301
2. Hu K.S., Xiao X., CaO X.F, Hao R., Zuo X.X., Zhang X.J., Nan J.M., *J. Hazard. Mater*. 192 (2011) 514.
3. Anderson C., Bard A.J., *J.Phys. Chem*. 99 (1995) 9882.
4. Chen X., Mao S.S., *Chem. Rev*. 107 (2007) 2891.
5. Fujishima A., Rao T.N., Tryk D.A., *J. Photochem. Photobiol. C: Photochem. Re.* 1 (2000) 11.
6. Peng T., Zhao D., Dai K., Shi W., Hirao. K., *J. Phys. Chem .B.* 109 (2005) 4947.
7. Zhao J., Wu T., Wu K., Oikawa K., Hidaka H., Serpone N., *Environ. Sci. Technol*. 32 (1998) 2394.
8. Torimoto T., Ito S., Kuwabata S., Yoneyama H., *Environ. Sci.Technol*. 30 (1996) 1275.
9. Xu Y., Langford C.H., *J. Phys. Chem*. 99 (1995) 11501.
10. Kalathil S., Mansoob Khan M., Ansari S.A., Lee J., Cho M.H., *Nanoscale*. 5 (2013) 6323.
11. Mansoob Khan M., Ansari S.A., Pradhan D., Omaish Ansari M., Han D.H., Lee J., Cho. M.H., *J. Mater. Chem. A.* 2 (2014) 637.
12. Mokhtar Mohamed M., *Appl. Catal. A Gen*. 267 (2004) 135.
13. Abdennouri M., Elmoubarki R., Elmhammedi A., Galadi A., Baalala M., Bensitel M., Boussaoud A., El hafiane Y., Smith A., Barka N., *J. Mater. Environ. Sci*. 4 (2013) 953.
14. Gyorgy E., Axente E., Mihailescu I.N., Ducu C., Duc H., *Appl. Surf. Sci*. 252 (2006) 4578.
15. Karthik K., Kesava Pandian S., Victor Jaya N., *Appl. Surf. Sci.* 256 (2010) 6829.
16. Tseng H.H., Wei M.C., Hsiunga S.F., Chioua C.W., *Chem. Eng. J*. 150 (2009) 160.
17. Gomathi Devi L., Narasimha Murthy B., Girish Kumar S., *Chemosphere*. 76 (2009) 1163.
18. Du Y., Gan Y., Yang P., Cuie Z., Hua.N., *Chem. Phys*. 103 (2007) 446.
19. Mansoob M., Khan J., Lee Cho M.H., *J. Ind. Eng. Chem*. 20 (2014) 1584.
20. Ishibai Y., Sato J., Akita S., Nishikawa T., Miyagishi S., *J. Photochem. Photobiol*. *A: Chem*. 188 (2007) 106.
21. Murakami Y., Ohta I., Hirakawa T., Nosaka Y., *Chem. Phys. Lett*. 493 (2010) 292.
22. Akpan U.G., Hameed B.H., *Appl. Catal. A Gen*. 375 (2010) 1.
23. Ansari S.A., Mansoob Khan M., Ansari M.O., Cho M.H., *Ceram. Int*. 41 (2015) 9131- 9139.
24. Hench LL., *J Am Ceram Soc*. 74 (1991) 1487.
25. Takagi O., Kuramoto N., Ozawa M., Suzuki S., *Ceramics international*. 30 (2004) 139.
26. Wei W., Sun R., Cui J., Wei Z.G., *Desalination*. 263 (2010) 89.
27. Chen S.B., Ma Y.B., Chen L., Xian K., *Geochemical Journal*. 44 (2010) 233.
28. Peltola T., Patsi M., Rahiala H., Kangasniemi I., Yli-Urpo A., *J Biomed Mater Res*. 41 (1998) 504.
29. Kaneda K., Mori K., Hara T., Mizugaki T., Ebitani K., *Cat Surv Asia.* 8 (2004) 231.
30. Nonami T., Taoda H., Hue N.T., Watanabe E., Iseda K., Tazawa M., et al. *Mater Res Bull*. 33 (1998) 125.
31. Wu W.J., George H.N., *J Colloid Interf Sci*. 2 (1998) 206.
32. So W.W., Park S.B., Kim K.J., Moon S.J., *J Colloid Interf Sci*. 191 (1997) 398.
33. Joseph Nathanael A., Mangalaraj D., Pao Chi Chen, Ponpandian N., *J Composites Science and Technology*. 70 (2010) 419.
34. Ahmad A., Awan G. H., Aziz S., *Pakistan Engineering Congress, in: 70th Annual Session Proceedings*. (1999) 404.
35. Liao C.J., Lin F.H., Chen K.S., Sun J.S., *Biomaterials 20* (1999) 1807.
36. Hongquan Z., Yuhua Y., Youfa W., Shipu L., *Mater Res*. 6 (2003) 111.
37. So W.W., Park S.B., Kim K.J., Moon S.J., *J Colloid Interf Sci*. 191 (1997) 398.
38. Sujaridworakun P., Koh F., Fujiwara T., Pongkao D., Ahniyaz A., Yoshimura M., *Mater. Sci. Eng. C.* 25 (2005) 87.
39. Pratap Reddy M., Venugopal A., Subrahmanyam M., *Appl Catal B: Environ*. 69 (2007) 164.
40. Nezamzadeh-Ejhieh A., Salimi Z., *Appl. Catal. A: Gen*. 390 (2010) 110.